

# Dynamics of dinuclear system formation and its decay in heavy ion collisions

Avazbek Nasirov<sup>1,2</sup>, Giorgio Giardina<sup>3</sup>, Giuseppe Mandarglio<sup>3</sup>,  
Marina Manganaro<sup>3</sup>, Werner Scheid<sup>4</sup>

<sup>1</sup>Joint Institute for Nuclear Research, 141980 Dubna, Russia

<sup>2</sup>Institute of Nuclear Physics, 100214, Tashkent, Uzbekistan

<sup>3</sup>Dipartimento di Fisica dell' Università di Messina, 98166 Messina, and Istituto Nazionale di Fisica Nucleare, Sezione di Catania, Italy

<sup>4</sup>Institute für Theoretische Physik der Justus-Liebig-Universität, Giessen, Germany

E-mail: nasirov@jinr.ru

**Abstract.** A variety of phenomena connected with the formation of a dinuclear complex is observed in the heavy ion collisions at low energies. The dinuclear system model allows us to analyze the experimental data and to interpret them by comparison of the partial capture, fusion and evaporation residue cross sections measured for the different reactions leading to the same compound nucleus. The comparison of theoretical and experimental values of the mass and angular distributions of the reaction products gives us a detailed information about reaction mechanism forming the observed yields. The observed very small cross sections of the evaporation residues may be explained by the strong fusion hindrance and/or instability of the heated and rotating compound nucleus and smallness of its survival probability. The fusion hindrance arises due to competition between complete fusion and quasifission while the smallness of survival probability is connected with the decrease of the fission barrier at large excitation energy and angular momentum of compound nucleus.

## 1. Introduction

In the heavy ion collisions at low energies, a variety of phenomena is observed, which are connected with the formation of a dinuclear complex. Deeply inelastic collisions have been studied extensively over a wide range of energies and masses [1]. The multinucleon transfer and energy dissipation mechanisms of these reactions are very similar with the ones of the full momentum transfer (capture) reactions. The difference between deep inelastic collisions and quasifission reactions is determined by the lifetimes of the dinuclear system (DNS) formed as intermediate system which consists of interacting nuclei with indestructible cores and excited nucleons in high-lying quantum states. Some of these excited nucleons form the neck or overlap region between constituents of DNS. The nucleon exchange mechanism at dissipation of the relative motion energy of the colliding nuclei was theoretically studied in Ref.[2, 3]. The basic points of those methods were developed to study deep inelastic and quasifission processes which are used to explain the hindrance to complete fusion [4].

The set of the successful experimental results in the synthesis of superheavy elements stimulated great efforts to experimental and theoretical investigations of the fusion-fission processes with massive nuclei. The very small cross sections  $\sigma_{ER}$  of the evaporation residues

observed in the recent experiments [5, 6, 7] may be explained by the strong fusion hindrance and/or instability of the heated and rotating compound nucleus [8].

The experimental knowledge about fusion-fission reactions at sub- and near-barrier energies has grown considerably in the last twenty years. The theoretical models are able to reproduce the main features of such processes, even to make predictions of the cross sections for synthesis of superheavy elements which are more or less close to the experimental data. But properly understanding the fusion dynamics for heavy systems requires many more ingredients. The necessity of more experimental data to disentangle various concurrent effects, is clearly felt. A full understanding of all steps of the reaction dynamics is very important for the challenging issue of superheavy element production and new isotopes far from the valley of stability.

Dynamics of complete fusion and role of the entrance channel in formation of the reaction products in heavy ion collisions are questionable or they have different interpretation still nowadays. For example, what mechanism of fusion makes the main contribution to formation of compound nucleus: an increase of the neck between interacting nucleus or multinucleon transfer at a relatively restricted neck size? How large is the overlap between angular momentum distributions of dinuclear system and compound nucleus which determine the angular distribution of reaction products, cross sections of evaporation residue, fusion-fission and quasifission products? There is an ambiguity in separation of fusion-fission fragments from the quasifission and fast fission products. Still unclear surely a law of the distribution of the excitation energy of DNS between its constituent fragments. Therefore, it is interesting to study the mechanism of deep inelastic and quasifission reactions forming binary fragments accompanied by neutron and gamma quantum emissions. The analysis of a correlation angular, mass-energy distributions of the registered fragments and neutron and gamma quantum characteristics allows us to obtain useful knowledge about the complete fusion mechanism.

## 2. Difference and similarity of quasifission and deep inelastic reactions

An investigation of dissipation dynamics of the deep inelastic and quasifission reactions is useful to establish relaxation times of different degrees of freedom in heavy ion collisions at low energies. From an analysis of the experimental data of the mass-angle distributions of the binary reaction products and gamma-quanta of giant dipole resonances we can conclude that a study of the DNS stage of these dissipative processes is perspective. Because a sufficient part of the reaction time of the dissipative processes in heavy ion collisions belongs to this stage, particularly for the massive system, as well as for the case of colliding nuclei with nearly equal charge (mass) numbers. Qualitative difference between deep inelastic and quasifission reactions is that the full momentum transfer does not take place in the former mechanism while it occurs in the latter one. The classification of the experimental data of binary products as ones corresponding to the deep inelastic collision or capture reactions (quasifission and fusion-fission) is based on the mass distribution characteristics only: projectile-like and target-like products with the total kinetic energies (TKE) around the Viola systematics [9] are considered as products of deep inelastic collisions. The authors of Ref. [10] attributed all events with energy losses larger than 8–15 MeV and with fragments of below 40 mass units to deep inelastic collision at the analysis of the experimental data of the  $^{32}\text{S}+^{182}\text{W}$  reaction.

The capture, deep inelastic and complete fusion reaction cross sections are presented in Fig. 1. The difference between capture and complete fusion cross sections is the quasifission cross section:

$$\sigma_{\text{cap}} = \sigma_{\text{fus}} + \sigma_{\text{qfis}}. \quad (1)$$

Unfortunately, a possibility of the mixing mass-angle distributions of the quasifission and deep inelastic reactions is not studied well because the nature of quasifission has been not established yet.

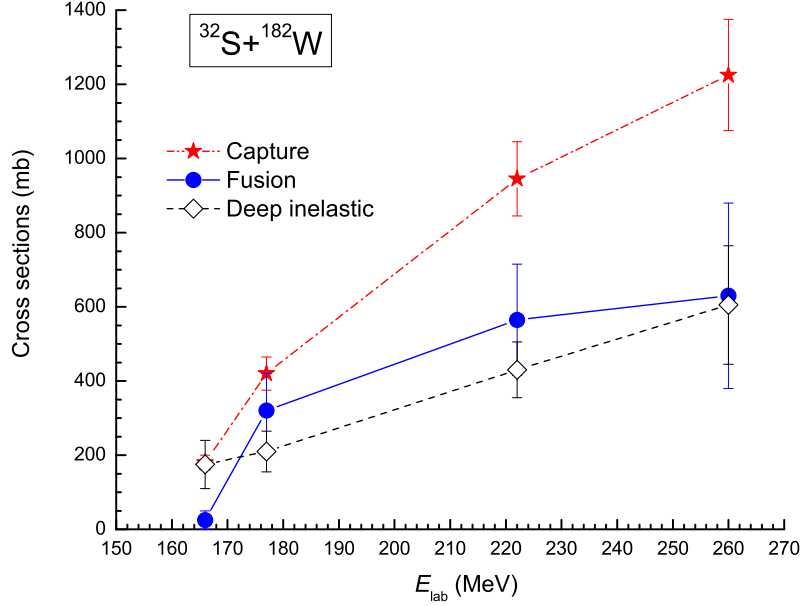


**Figure 1.** The experimental data for capture (dot-dashed line), complete fusion (solid line) and deep inelastic collision (dashed line) events for the  $^{32}\text{S}+^{182}\text{W}$  reaction [10].

The difference between capture and deep inelastic reactions can be found theoretically from the analysis of the results of dynamical calculations by solving the equations of motion for the radial distance (Eq. 2), angular momentum (Eq. 6) and surface vibrations for quadrupole and octupole multipolarity (Eq. 4) (see Fig. 2) for the  $^{48}\text{Ca}+^{208}\text{Pb}$  reaction.

The quasifission occurs at the full momentum transfer and it belongs to the capture reactions when the system traps into potential well as in Fig. 2(a) and the decay time of DNS, which is formed in this mechanism, is determined by the size of the potential well, by the values of excitation energy  $E_{\text{DNS}}^*$  and friction coefficients (radial and tangential).

In the deep inelastic reactions, the DNS is not trapped into the potential well because the DNS momentum decreases up to zero and the relative distance between centers of mass of projectile and target nuclei reaches the minimum value (see Fig. 2(b)). Then the relative distance  $R$  increases due to repulsive forces. Although the kinetic energy of the relative motion goes on to be dissipated the DNS can overcome the Coulomb barrier from intrinsic part to outside of the potential well and we observe two products after interaction and exchanging nucleons. Therefore, the interaction time of colliding nuclei in deep inelastic collision is small in comparison with the one in capture reactions. The friction coefficients and the size of the potential well play a crucial role in the calculations of capture events by solving the following equations [4, 11]:

$$\mu(R, \alpha_1, \alpha_2)\ddot{R} + \gamma_R(R, \alpha_1, \alpha_2)\dot{R}(t) = F(R), \quad (2)$$

$$F(R, \alpha_1, \alpha_2) = -\frac{\partial V(R, \alpha_1, \alpha_2)}{\partial R} - \dot{R}^2 \frac{\partial \mu(R)}{\partial R}, \quad (3)$$

$$D_{\beta_i}\ddot{\beta}_i(t) + \gamma_{\beta}(R)\dot{\beta}_i(\alpha_1, \alpha_2, t) = F_{\beta_i}(R) \quad (4)$$

$$F_{\beta}(R) = -\frac{\partial V(\beta_i, \alpha_1, \alpha_2)}{\partial \beta_i} \quad (5)$$

$$\frac{dL}{dt} = \gamma_{\theta}(R, \alpha_1, \alpha_2)R(t) \left( \dot{\theta}R(t) - \dot{\theta}_1 R_{1eff} - \dot{\theta}_2 R_{2eff} \right), \quad (6)$$

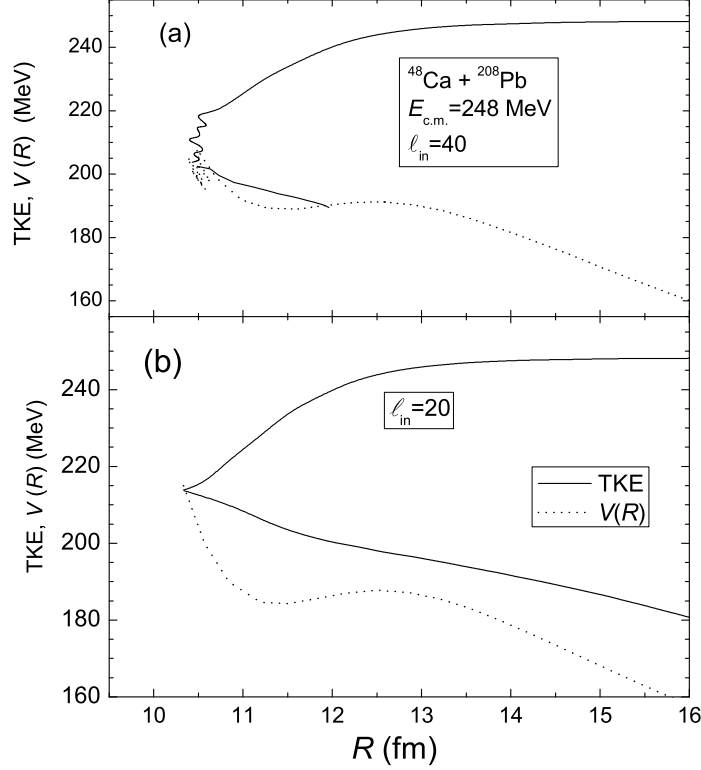


**Figure 2.** Capture (a) and deep inelastic collision (b) for the  $^{48}\text{Ca}+^{208}\text{Pb}$  reaction.

$$L_0 = J_R(R, \alpha_1, \alpha_2)\dot{\theta} + J_1\dot{\theta}_1 + J_2\dot{\theta}_2, \quad (7)$$

$$E_{\text{rot}} = \mu(R, \alpha_1, \alpha_2)\dot{R}^2/2 + \frac{J_R(R, \alpha_1, \alpha_2)\dot{\theta}^2}{2} + \frac{J_1\dot{\theta}_1^2}{2} + \frac{J_2\dot{\theta}_2^2}{2}, \quad (8)$$

where  $R \equiv R(t)$  is the relative motion coordinate;  $\dot{R}(t)$  is the corresponding velocity;  $\alpha_1$  and  $\alpha_2$  are the orientation angles between beam direction and axial symmetry axis of the projectile and target, respectively;  $L_0$  ( $L_0 = \ell_0\hbar$ ) and  $E_{\text{rot}}$  are defined by initial conditions;  $J_R$  and  $\theta$ ,  $J_1$  and  $\theta_1$ ,  $J_2$  and  $\theta_2$  are moment of inertia and angular velocities of the DNS and its fragments, respectively;  $\gamma_R$  and  $\gamma_\theta$  are the friction coefficients for the relative motion along  $R$  and the tangential motion when two nuclei roll on each other's surfaces, respectively;  $\omega_\lambda^{(i)}$ ,  $\gamma_\lambda$  and  $D_\lambda^{(i)}$  are frequency, damping and mass coefficients for the surface vibrations with multipolarity  $\lambda$ , respectively;  $V(R, \alpha_1, \alpha_2)$  is the nucleus-nucleus potential calculated by the double folding procedure [4, 12].

The capture includes complete fusion and quasifission events. The quasifission time is estimated by the formula

$$\tau_{\text{DNS}}(T_Z) = \frac{\hbar}{\Gamma_{\text{qfiss}}(T_Z)} \quad (9)$$

if we know the excitation energy  $E_{\text{DNS}}^*$  and quasifission barrier  $B_{\text{qf}}$  of the dinuclear system for its decay in fragments with charge numbers  $Z$  and  $Z_{\text{tot}} - Z$ , by using the one-dimensional Kramers rate [13, 14, 15]

$$\begin{aligned} \Gamma_{\text{qfiss}}(\Theta) &= K_{\text{rot}}^{(\text{DNS})}/K_{\text{rot}}^{(\text{CN})} \omega_m \left( \sqrt{\gamma^2/(2\mu_{\text{qf}})^2 + \omega_{\text{qf}}^2} - \gamma/(2\mu_{\text{qf}}) \right) \\ &\times \exp(-B_{\text{qf}}/T_Z) / (2\pi\omega_{\text{qf}}). \end{aligned} \quad (10)$$

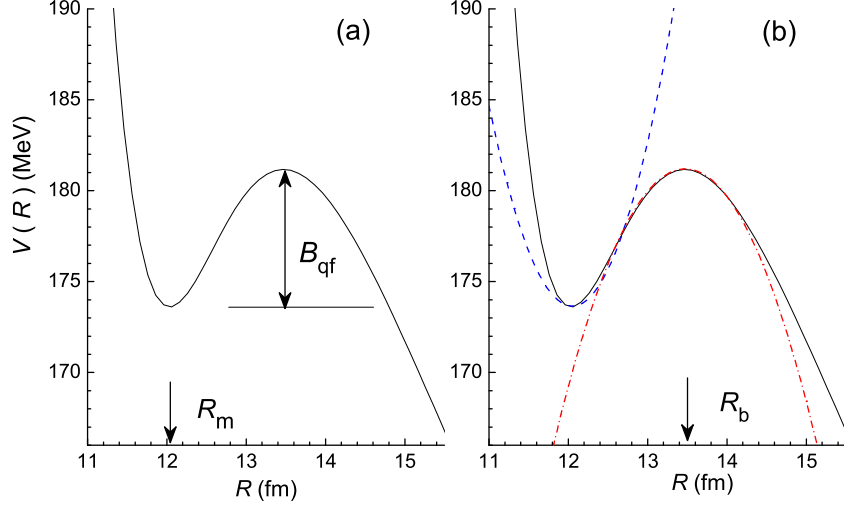


**Figure 3.** (a) Quasifission barrier is the depth of the well in the nucleus-nucleus interaction potential  $V(R)$ . (b) The potential well is replaced by the harmonic oscillator with frequency  $\omega_m$  and the potential barrier is replaced by the inverted harmonic oscillator with frequency  $\omega_b$  which are used to calculate the decay time of DNS into two fragments.

Here the frequencies  $\omega_m$  and  $\omega_b$  are found by the harmonic oscillator approximation to the shape of the nucleus-nucleus potential  $V(R)$  for a given DNS configuration  $(Z, Z_{\text{tot}} - Z)$  on the bottom of its pocket placed at  $R_m$  and on the top (quasifission barrier) placed at  $R_b$  (see Fig. 3), respectively:

$$\omega_m^2 = \mu_{\text{qf}}^{-1} \left. \frac{\partial^2 V(R)}{\partial R^2} \right|_{R=R_m}, \quad (11)$$

$$\omega_b^2 = \mu_{\text{qf}}^{-1} \left. \frac{\partial^2 V(R)}{\partial R^2} \right|_{R=R_b}. \quad (12)$$

The nucleus-nucleus potential  $V(Z, A, \ell, R)$  includes the Coulomb  $V_{\text{Coul}}(Z, A, R)$ , nuclear  $V_{\text{N}}(Z, A, R)$  and rotational  $V_{\text{rot}}(Z, A, R, \ell)$  parts:

$$V(Z, A, \ell, R) = V_{\text{Coul}}(Z, A, R) + V_{\text{N}}(Z, A, R) + V_{\text{rot}}(Z, A, R, \ell), \quad (13)$$

where  $R$  is the distance between the centers of the nuclei. Details of the calculation can be found in Refs. [16, 17].

The calculated values of  $\hbar\omega_m$  and  $\hbar\omega_b$  were equal to 46.52 MeV and 22.37 MeV, respectively. The used value of the friction coefficient  $\gamma$  is equal to  $8 \cdot 10^{-22}$  MeV fm $^{-2}$ s which was found from our calculations;  $\mu_{\text{qf}} \approx \mu = A_1 \cdot A_2 / A_{\text{CN}}$ , where  $A_1$  and  $A_2$  are the mass numbers of the quasifission fragments.

The collective enhancement factor  $K_{\text{rot}}$  of the rotational motion to the level density should be included because the dinuclear system is a good rotator. It is calculated by the well known expression [18]:

$$K_{\text{rot}}(E_{\text{DNS}}) = \begin{cases} (\sigma_{\perp}^2 - 1)f(E_{\text{DNS}}) + 1, & \text{if } \sigma_{\perp} > 1 \\ 1, & \text{if } \sigma_{\perp} \leq 1, \end{cases}$$

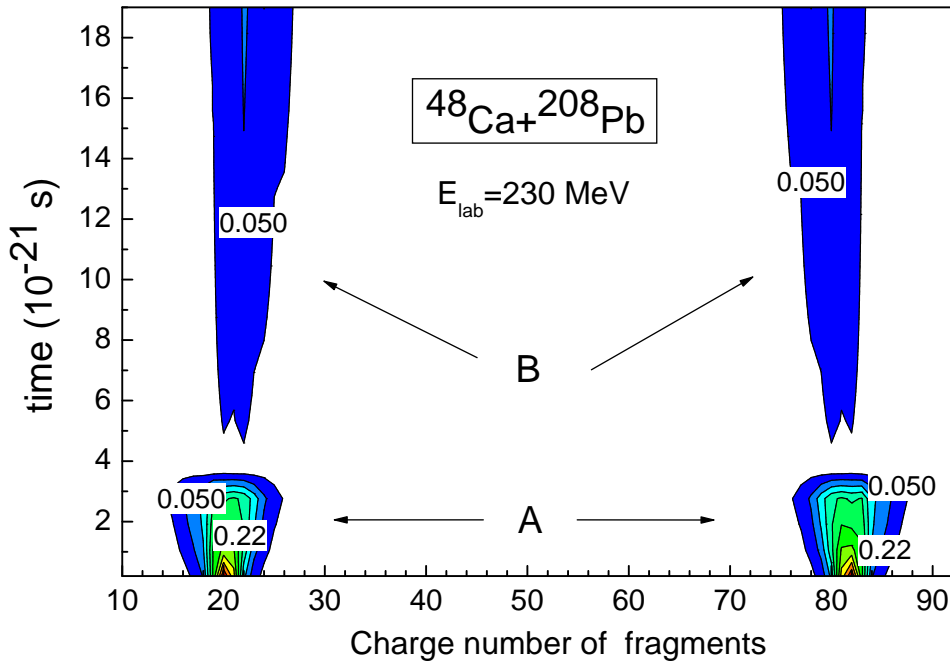


**Figure 4.** Time dependence of the charge distribution of deep inelastic collision (A) and quasifission (B) products for the  $^{48}\text{Ca} + ^{208}\text{Pb}$  reaction.

where  $\sigma_{\perp}^2 = J_{\perp}^{(\text{DNS})} T / \hbar^2$ ;  $f(E) = (1 + \exp[(E - E_{\text{cr}})/d_{\text{cr}}])^{-1}$ ;  $E_{\text{cr}} = 120\tilde{\beta}_2^2 A^{1/3}$  MeV;  $d_{\text{cr}} = 1400\tilde{\beta}_2^2 A^{2/3}$ .  $\tilde{\beta}$  is the effective quadrupole deformation for DNS. We find it from the value of the DNS moment of inertia relative to rotation around axis perpendicular to the line connecting the mass centers of nuclei which is calculated by the formula:

$$\mathcal{J}_{\perp}^{\text{DNS}} = \mathcal{J}_1 + \mathcal{J}_2 + M_1 d_{\perp}^{(1)2} + M_2 d_{\perp}^{(2)2}, \quad (14)$$

where  $d_{\perp}^{(i)}$  is the distance between the center of mass of the fragment  $i$  ( $i = 1, 2$ ) and the line corresponding to the largest moment of inertia of DNS (see Fig. 11 in Ref.[19]).

The DNS can have a long lifetime ( $\tau_{\text{DNS}}$ ) if it is formed at capture: the value of  $\tau_{\text{DNS}}$  depends on the depth of the potential well ( $B_{\text{qf}}$ ), DNS excitation energy ( $E_{\text{DNS}}^*$ ) at the given value of angular momentum  $\ell$  and its moment of inertia  $\mathcal{J}_{\perp}^{\text{DNS}}$  [19].

Due to the shell effects as the quantum states of the neutron and proton systems of the interacting nuclei we have the DNS as a molecule of nuclei which does not fuse immediately. Therefore, the peculiarities of the DNS stage influences on formation of the reaction products with magic proton or neutron numbers. Shell effects are observed as cluster states in the large amplitude collective motions of nuclei. The observed cluster emission, mass-charge distribution of the quasifission fragments and spontaneous asymmetric fission of Th, U and Cf isotopes proved the strong role of shell structure. Reactions of heavy ion collisions and fission (spontaneous and induced) processes can be studied well using the DNS concept.

A characteristic feature of the deep inelastic processes is that the target and projectile identity is largely preserved. In Ref. [20], only for low TKE of the outgoing products (energies below the Coulomb repulsion,  $V_C$ , of touching spheres) a small mass drift is found. In these studies, it was difficult to establish the magnitude of such a drift unambiguously, because a relatively small initial mass asymmetry made it difficult to separate drifting projectile- and target-like distributions from the wings of a mass symmetric component.

We would like to stress the importance to distinguish the scattering processes, with no or negligible mass drift, i.e. quasi- and deep inelastic processes, from capture reactions that exhibit a small or large mass drift, usually but not always going to the full mass symmetry configuration and leading to decay into two almost equally large fragments.

The analysis of the mass (charge) distribution of the binary reaction products showed in Refs. [20] and [21, 22] shows that in collisions of nuclei with magic proton or/and neutron numbers at a charge or mass drift around Coulomb barrier energies may be small in capture reactions too. In Ref. [20], an averaged charge number of the projectile-like products  $^{86}\text{Kr} + ^{166}\text{Er}$  was equal

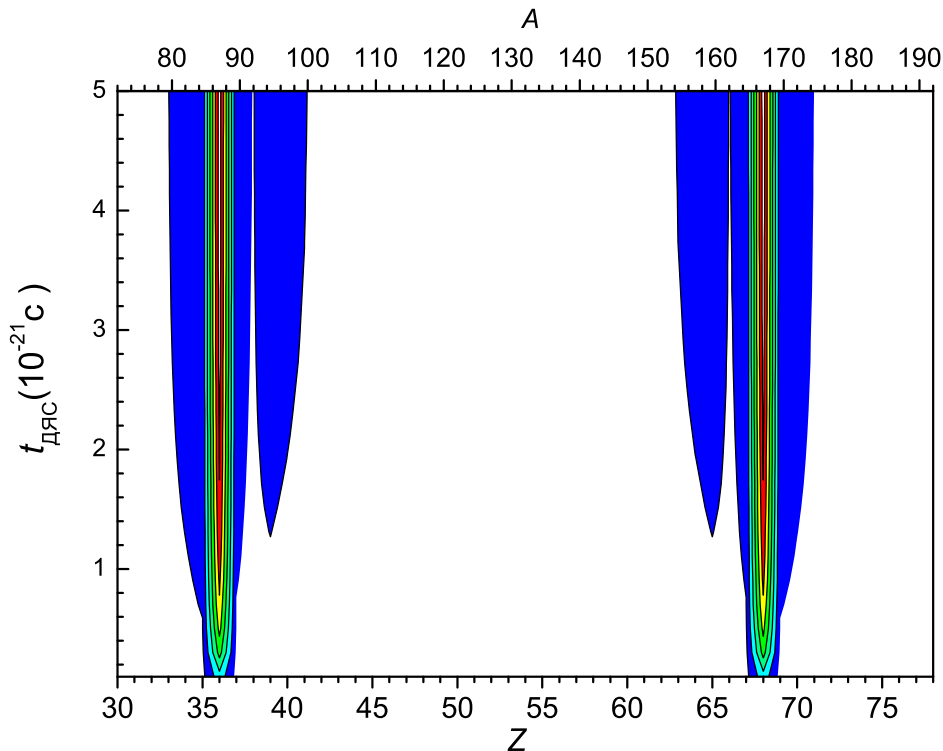


**Figure 5.** Time dependence of the charge distribution of deep inelastic collision and quasifission products for the  $^{86}\text{Kr} + ^{166}\text{Er}$  reaction.

to the initial value  $\langle Z_{\text{PLF}} \rangle = 36$  up to the total kinetic energy (TKE) loss of 180 MeV. Our theoretical results presented in Fig.5 show that deep inelastic and quasifission reactions products are mixed having the same charge number because the driving potential has a minimum at  $Z = 36$  corresponding to the projectile charge number. A similar phenomenon was observed in the  $^{48}\text{Ca} + ^{208}\text{Pb}$  reaction [22]. The small drift from the initial charge number of the projectile-like products does not mean that the deep inelastic reactions occurred only. A maximum of the charge distribution can be concentrated at the charge value corresponding to the minimum of the potential energy surface. This phenomenon was reproduced by the DNS model and our results of the charge and mass distributions of the deep inelastic collisions (A) and quasifission (B) fragments are presented in Fig.4.

Understanding the mass drift is basic for the investigation of the reaction mechanism. It is relevant to the deep inelastic processes and to the capture processes. In capture reactions with heavy nuclei, the direction of the mass drift could influence the probability for the compound nucleus formation: a drift towards asymmetry could favor true compound nucleus formation (with subsequent evaporation of neutrons leading to the observed evaporation residues or fission fragments), whereas a drift towards symmetry could favor quasifission without compound nucleus formation.

### 3. Difference between capture and complete fusion for light and massive systems

For light or medium-heavy systems, capture inside the Coulomb barrier leads to complete fusion, so that the capture (or barrier-passing) cross section may be equal to the complete fusion cross-section. According to the DNS concept the hindrance to complete fusion is connected with the presence of the quasifission process as a competing channel which leads to formation of

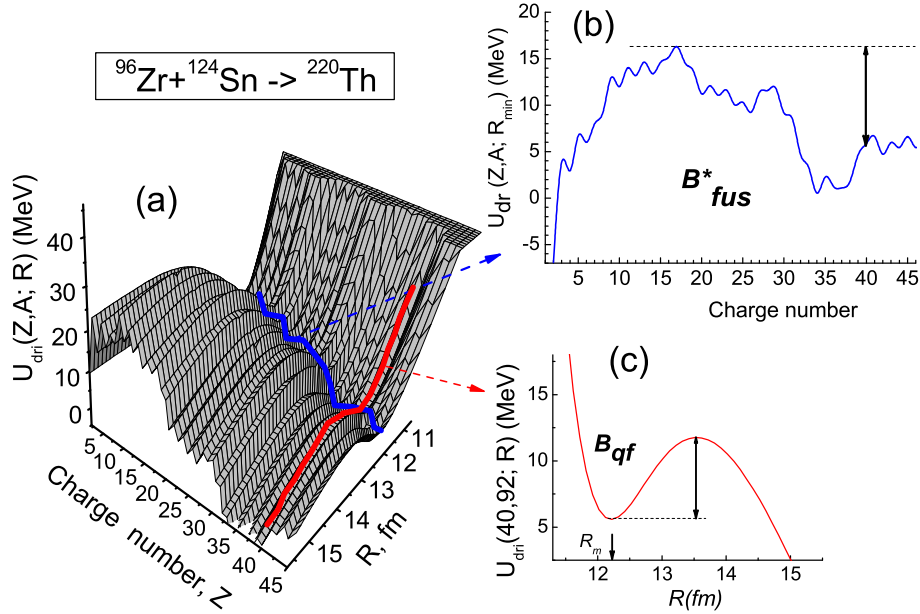


**Figure 6.** Potential energy surface calculated for the DNS formed in the  $^{96}\text{Zr}+^{124}\text{Sn} \rightarrow ^{220}\text{Th}$  reaction (a); driving potential built by connection of minima of the potential wells for all values of charge asymmetry of DNS (b):  $B_{\text{fus}}^*$  is considered as the intrinsic fusion barrier for the transformation of the DNS from the configuration with the charge asymmetry  $Z = 40$ ; potential well with depth  $B_{\text{qf}}$  which is used as the quasifission barrier (c). The minimum value of the potential well is at  $R = R_m$ .

binary products without formation of the compound nucleus [4, 12]. For the analysis and study of the hindrance to complete fusion we calculate the potential energy surface for DNS formed during the interaction of the nuclei as the sum of the reaction energy balance ( $Q_{\text{gg}}$ ) and the nucleus-nucleus interaction  $V(R)$ :

$$U_{\text{driv}}(Z_1, R, \ell) = Q_{\text{gg}} + V(R), \quad (15)$$

where  $Q_{\text{gg}} = B_1 + B_2 - B_{\text{CN}}$ ;  $B_1$ ,  $B_2$  and  $B_{\text{CN}}$  are the binding energies of the constituents of the DNS and compound nucleus, respectively. The values of the binding energies are obtained from [23, 24]. The evolution of DNS with given initial charge numbers of projectile- and target-nucleus ( $Z_P$  and  $Z_T$ ) is determined by the potential energy surface. As an example, the potential energy surface calculated for the  $^{96}\text{Zr}+^{124}\text{Sn}$  reaction is presented in Fig. 6(a). The approaching path of the projectile to the target nucleus occurs along the  $R$ -axis which is the distance between mass centers of colliding nuclei. Overcoming the Coulomb barrier the system starts to lose its kinetic energy of relative motion due to particle-hole excitation of nucleons and nucleon exchange as it is shown in Fig. 2. In this Section and further we consider capture reactions when a full momentum transfer in heavy ion collisions occurs. The evolution of DNS along charge asymmetry takes place along the valley on the potential energy surface. The driving potential  $U_{\text{driv}}$  is the curve lying on the bottom of this valley. A presence of a hindrance to complete fusion by multinucleon transfer can be found by an estimation of the intrinsic fusion barrier  $B_{\text{fus}}^*$  as the difference between a values of  $U_{\text{driv}}$  corresponding to the initial charge asymmetry and its maximum value to the way of complete fusion  $B_{\text{fus}}^*(Z_P) = U_{\text{driv}}(Z_{\text{max}}) - U_{\text{driv}}(Z_P)$ . For

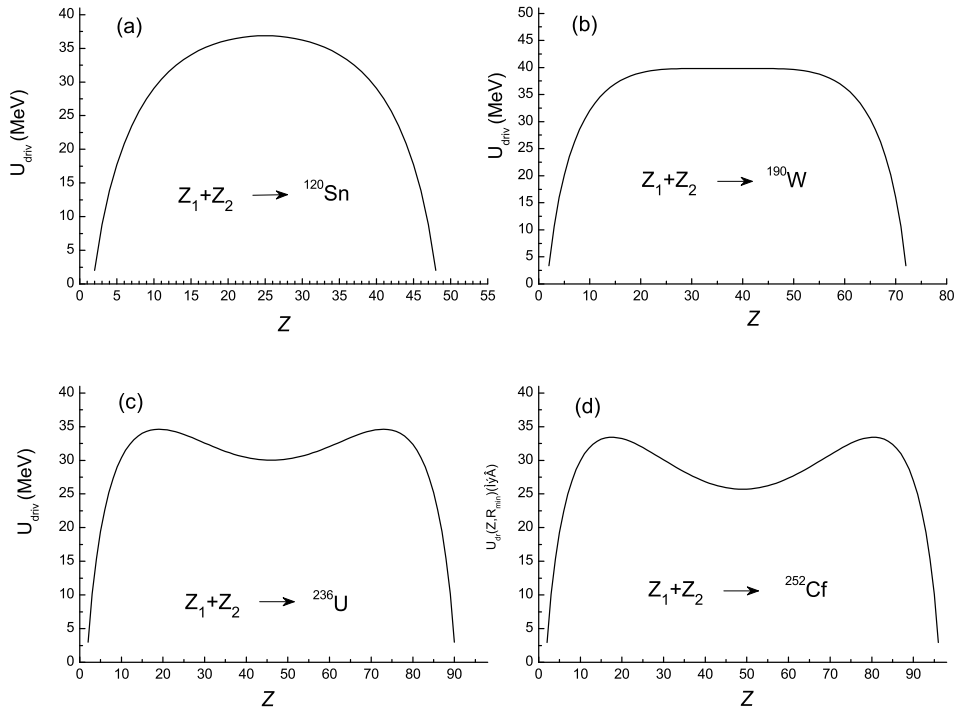


**Figure 7.** Driving potentials calculated for the DNS leading to formation of the compound nuclei  $^{120}\text{Sn}$  (a),  $^{190}\text{W}$  (b),  $^{236}\text{U}$  (c) and  $^{252}\text{Cf}$  (d).

example, in Fig. 6(b),  $B_{\text{fus}}^*(Z_P)=10.2$  MeV, because  $U_{\text{driv}}(17) = 16$  and  $U_{\text{driv}}(40) = 5.8$  MeV. The quasifission barrier  $B_{\text{qf}}$  for the charge asymmetry  $Z_P = 40$  is equal to 5.68 MeV. The excitation energy of the DNS  $E_{\text{DNS}}^* = E_{\text{c.m.}} - V(R_m) + \Delta Q_{\text{gg}}$ , as well as  $B_{\text{fus}}^*$  and  $B_{\text{qf}}$  determine a hindrance to complete fusion.

Taking into account the dependence of the hindrance to complete fusion on the orbital angular momentum  $\ell$  we calculate partial fusion cross section as a function of the collision energy  $E_{\text{c.m.}}$  [4, 12, 17]:

$$\sigma_{\text{fus}}^{(\ell)}(E_{\text{c.m.}}) = \sigma_{\text{cap}}^{(\ell)}(E_{\text{c.m.}})P_{\text{CN}}^{(\ell)}(E_{\text{c.m.}}), \quad (16)$$

$P_{\text{CN}}^{(\ell)}$  is the fusion probability in competition between complete fusion and quasifission. For light systems the capture and complete fusion cross sections are equal because  $P_{\text{CN}}^{(\ell)} = 1$  for the values of  $\ell$  for which the intrinsic fusion barrier  $B_{\text{fus}}^*$  is equal to zero. To see a dependence of the fusion probability on the total charge and mass numbers of the colliding nuclei we compare the driving potentials ( $\ell = 0$ ) which were calculated by the use of the liquid-drop model to obtain the binding energies  $B_1$ ,  $B_2$ , and  $B_{\text{CN}}$  for the four reactions leading to the compound nuclei  $^{120}\text{Sn}$ ,  $^{190}\text{W}$ ,  $^{236}\text{U}$  and  $^{252}\text{Cf}$  (see, Fig. 7). One can say that for all reactions leading to the CN  $^{120}\text{Sn}$  there is no hindrance to complete fusion because the maximum value of  $U_{\text{driv}}$  is at  $Z_1 = Z_2$ . Therefore, there is no intrinsic fusion barrier,  $B_{\text{fus}}^*=0$ . For the reactions leading to the CN  $^{190}\text{W}$  it is seen that approximately  $B_{\text{fus}}^*=0$ , but there is the plateau at  $20 < Z < 50$  which can be transformed to a hollow at large values of angular momentum. As a result we can observe a hindrance to complete fusion for colliding energies  $E_{\text{c.m.}}$  near and above the Coulomb barrier. The dependence of the driving potential on the DNS angular momentum for the reactions leading to the CN  $^{190}\text{W}$  is demonstrated in Fig. 8. The increase of  $\ell$  leads to decrease the middle charge

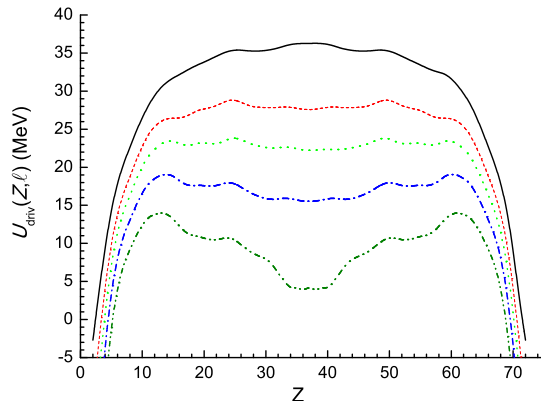


**Figure 8.** The dependence of the driving potential on the DNS angular momentum  $\ell_{\text{DNS}}$  for the reactions leading to the CN  $^{190}\text{W}$ :  $\ell = 0$  (solid line), 40 (dashed line), 60 (dotted line), 80 (dot-dashed line), and 100 (double dot-dashed line).

part ( $(Z_1 + Z_2)/2$  region) of the driving potential. Consequently, a hindrance to the complete fusion appears for the charge symmetric reactions leading to formation of  $^{190}\text{W}$  at large angular momentum. The increase of the hindrance by increasing the angular momentum for the massive systems was analyzed in Ref. [8].

#### 4. Cold and hot fusion mechanisms in the DNS model

The dynamics of complete fusion and the role of the entrance channel in the formation of heavy ion collision reactions are questionable or/and they have different interpretation still now. For example, what mechanism of fusion makes the main contribution to the formation of the compound nucleus: the increase of the radius of neck between interacting nuclei or multinucleon transfer at relatively restricted neck size? Priority of the proposed mechanism is determined by its possibility to explain different characteristics of the observed physical quantities using the same dynamical variables of the model. To show the advance of the DNS model we demonstrated the peculiarities of the angular momentum distribution of DNS and compound nucleus which determine the angular distribution of reaction products, cross sections of evaporation residue, fusion-fission and quasifission products. We are trying to improve this model to use it for the separation of fusion-fission fragments from the quasifission and fast fission products. It is well known that similarity of the mass and energy distributions of above mentioned processes causes difficulties at the analysis of the experimental data to establish the contribution of the every reaction mechanism into measured data. As well as this model can be applied to study distribution of the excitation energy between different degrees of freedom, as well as between reaction products.

In the DNS concept [25], the evaporation residue cross section at the collision energy  $E_{\text{c.m.}}$  is factorized as follows:

$$\sigma_{\text{ER}}(E_{\text{c.m.}}) = \sum_{\ell=0}^{\ell_f} \sigma_{\text{fus}}^{(\ell)}(E_{\text{c.m.}}) W_{\text{sur}}^{(\ell)}(E_{\text{c.m.}}), \quad (17)$$

where  $\sigma_{\text{fus}}^{(\ell)}$  is the partial cross section of the complete fusion of the projectile and target nuclei;  $W_{\text{sur}}^{(\ell)}$  is the survival probability against fission of the heated and rotating nucleus at each step of the de-excitation cascade by evaporation of neutrons, protons and light particles up to the

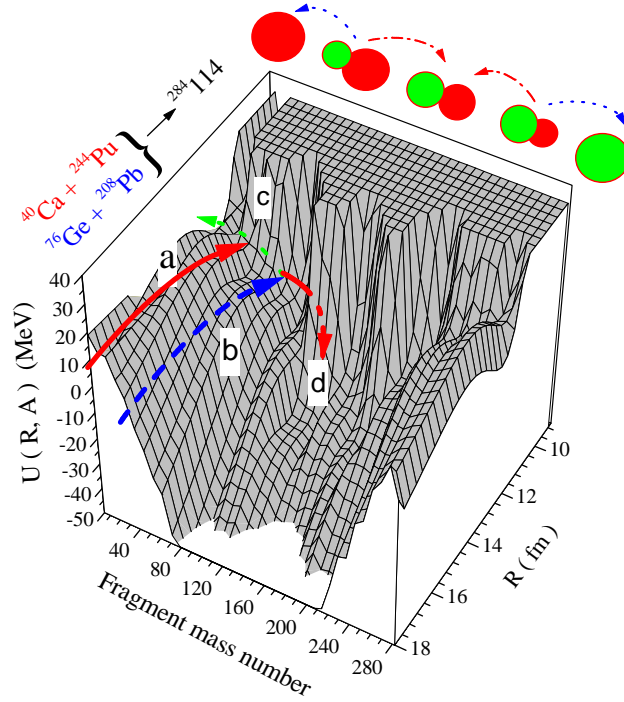


**Figure 9.** An explanation of the inevitable difference between excitation energies of the compound nucleus which can be formed in the “hot” ( $^{40}\text{Ca}+^{244}\text{Pu}$  –(a)) and “cold” ( $^{76}\text{Ge}+^{208}\text{Pb}$  – (b)) fusion reactions by the entrance channel and peculiarities of the potential energy surface. The arrows (c) and (d) show the complete fusion and quasifission directions, respectively.

formation of the evaporation residue;  $\ell_f$  is the value of CN angular momentum at which the fission barrier disappears:  $W_{\text{sur}}^{(\ell)}(E) = 0$  for  $\ell > \ell_f$ . The decrease of  $W_{\text{sur}}$  by increasing the excitation energy is determined by the increase of rate of competition between fission and emission of particles.

At the synthesis of the superheavy elements  $Z > 114$  the observed cross sections of the evaporation residues are near or less than 1 pb. The smallness of  $\sigma_{\text{fus}}$  or/and  $W_{\text{sur}}$  in formula (17) leads to small values of the measured cross section  $\sigma_{\text{ER}} \sim 1\text{pb}$ .

The experience of the synthesis of superheavy elements showed that the used reactions can be separated into “cold” and “hot” fusion reactions. In the “cold fusion” reactions the excitation energy the formed compound nucleus  $E_{\text{CN}}^*$  is less than 20 MeV [6, 7] while in “hot fusion” reactions  $E_{\text{CN}}^*$  is more than 25 MeV [5]. In the “cold fusion” reactions the evaporation residue nuclei are formed after emission 1 or 2 neutrons from the heated and rotating compound nucleus. In the “hot fusion” reactions the 3 or more neutron emission cascade precedes the evaporation residue formation. The charge asymmetry of the entrance channel determines the type of reaction: “cold fusion” reactions with the  $^{208}\text{Pb}$  and  $^{209}\text{Bi}$  targets used to synthesize superheavy elements Darmstadtium, Roentgenium and Copernicium are more mass symmetric than the “hot fusion” reactions with the  $^{48}\text{Ca}$  projectile on the actinide targets used to synthesize the heaviest elements  $Z = 114\text{--}118$  in the Flerov Laboratory of the Nuclear Reactions of Joint Institute for Nuclear Research. In Fig. 9, the arrow “a” shows the path of the entrance channel leading to the “hot fusion” reactions while the arrow “b” shows the path leading to “cold fusion” reactions. Due to peculiarities of the landscape of the potential energy surface for the massive system, the excitation energies of DNS and compound nucleus for the symmetric charge numbers (large reaction  $Q_{\text{gg}}$  values) are smaller in the entrance channel with the  $^{208}\text{Pb}$  target-nucleus (around arrow “b”):  $E_{\text{CN}}^* = E_{\text{c.m.}} + Q_{\text{gg}}$ . It is seen from the shape of the potential energy surface that the “hot fusion” reaction can not be made “colder” because the capture of projectile by the target-nucleus becomes impossible by decreasing the beam energy. Note, for

this system leading to formation of  $^{284}114$ , the “cold fusion” reaction  $^{76}\text{Ge}+^{208}\text{Pb}$  can not be made “warmer” because if we increase the beam energy significantly higher than the Coulomb barrier the system can not be captured due to the small size of the potential well in the nucleus-nucleus interaction and restricted value of the friction coefficient for radial motion: we observe only deep inelastic collisions as in Fig. 2(b). One can say that, for the “cold fusion” reaction, the increase of the beam energy enough higher than the Coulomb barrier does not lead to an increase of the fusion cross section as it is expected from the extra-extra push model [26]. In the “cold fusion” reactions with  $^{208}\text{Pb}$  and  $^{209}\text{Bi}$  targets an increase of the projectile charge number leads to the drastic hindrance to complete fusion as a result of the increase of contributions of the quasifission and deep inelastic collisions. This phenomenon explains the observed small cross section in the synthesis of superheavy element  $Z = 113$  in the  $^{64}\text{Zn}+^{209}\text{Bi}$  reaction [7].

**Table 1.** Comparison of the hindrance to formation of compound nucleus in the “cold” and “hot fusion” reactions used in the synthesis of superheavy elements.

“Cold fusion” reactions	$\eta = \frac{A_2-A_1}{A_1+A_2}$	$P_{\text{CN}}$	“Hot fusion” reactions	$\eta = \frac{A_2-A_1}{A_1+A_2}$	$P_{\text{CN}}$
$^{64}\text{Ni}+^{208}\text{Pb}^\dagger$	0.529	$1.4 \cdot 10^{-7}$	$^{48}\text{Ca}+^{244}\text{Pu}$	0.671	$4.96 \cdot 10^{-2}$
$^{64}\text{Ni}+^{209}\text{Bi}^\dagger$	0.531	$7.0 \cdot 10^{-8}$	$^{48}\text{Ca}+^{243}\text{Am}^\ddagger$	0.670	$5.02 \cdot 10^{-2}$
$^{70}\text{Zn}+^{208}\text{Pb}^\dagger$	0.496	$2.5 \cdot 10^{-9}$	$^{48}\text{Ca}+^{248}\text{Cm}^\ddagger$	0.676	$1.13 \cdot 10^{-2}$
$^{70}\text{Zn}+^{209}\text{Bi}^\dagger$	0.498	$5.2 \cdot 10^{-10}$	$^{48}\text{Ca}+^{249}\text{Bk}^\S$	0.677	$5.06 \cdot 10^{-3}$
$^{76}\text{Ge}+^{208}\text{Pb}^\dagger$	0.465	$1.2 \cdot 10^{-10}$	$^{48}\text{Ca}+^{249}\text{Cf}^\ddagger$	0.677	$7.14 \cdot 10^{-3}$

<sup>†</sup>The estimations from Ref.[4]

<sup>‡</sup>The estimations from Ref. [16]

<sup>§</sup>The estimations from Ref. [27]

In Fig. 10 we present a comparison of the ER cross sections obtained by the DNS model (dot-dashed line) with the experimental data for the synthesis of Roentgenium and Copernicium in the  $^{64}\text{Ni}+^{209}\text{Bi}$  and  $^{70}\text{Zn}+^{208}\text{Pb}$  reactions, respectively. The dashed and solid lines in Fig. 10 show the theoretical results for the quasifission and complete fusion excitation functions. The ratio of the complete fusion to capture excitation function ( $P_{\text{CN}}$ ) shows how strong is the hindrance to complete fusion (see Eq. (16)) due to the very small values of fusion cross section in comparison to the capture cross section. The event at  $E_{\text{CN}}^* = 9$  MeV in the  $^{70}\text{Zn}+^{208}\text{Pb}$  reactions (right panel) was described and published in [4] while the second event at  $E_{\text{CN}}^* = 12$  MeV was measured after the appearance of the cited paper. One can say that the second event was predicted in [4]. So, we conclude that the smallest cross section in the synthesis of Copernicium is caused mainly by the huge contribution of the quasifission events that is inherent for the “cold fusion” reactions. This conclusion was deduced from the theoretical analysis which included realistic nuclear shell effects in the calculation of the potential energy surface. The dotted lines in Fig. 10 show the fission barrier of the compound nucleus  $B_{\text{fis}}$  which is a function of its excitation energy and angular momentum.

The “hot fusion” reactions were favorable for the synthesis of the superheavy elements  $Z > 112$ : new superheavy elements  $Z = 114$ – $118$  have been obtained at the Flerov Laboratory of Nuclear Reactions of JINR (Dubna, Russia) [5] during the last decade. The ER cross sections in the synthesis of superheavy elements  $Z = 114$  and  $Z = 116$  were confirmed in the recent experiments performed in the Lawrence Berkeley Laboratory [28] and GSI (Darmstadt) [29], respectively. The main reason allowing the experimentalists to succeed in the “hot fusion”

reactions or the synthesis of the superheavy elements  $Z = 114$ – $118$  is smallness of the intrinsic fusion barrier  $B_{\text{fus}}^*$  which decreases the hindrance to complete fusion. But large values of the excitation energy and angular momentum of the compound nucleus formed in the “hot fusion” reactions decrease the survival probability against fission. Therefore, the cross sections of evaporation residues in synthesis of superheavy elements decreases from 3–4 picobarns for  $Z = 114$  up to 0.5 pb for  $Z = 118$ . In Table 1 we compare the hindrance for the formation of the compound nucleus in the “cold” and “hot fusion” reactions which were used in the synthesis of superheavy elements. The difference in the hindrances presented by  $P_{\text{CN}} = \sigma_{\text{fus}} / (\sigma_{\text{fus}} + \sigma_{\text{qfis}})$  in both types of reactions is evidently seen: i) the hindrance to complete fusion is stronger for the “cold fusion” reactions in comparison with “hot fusion” reactions; ii) the hindrance to “cold fusion” reactions increases drastically by increasing of the projectile charge number while it changes slowly in “hot fusion” reactions by increasing the target charge number. This is explained by a strong change of the potential energy surface around the charge asymmetry  $Z = 82(A = 208)$  and it has more sloping shape in the region  $Z = 20(A = 48)$  (see Fig. 9).

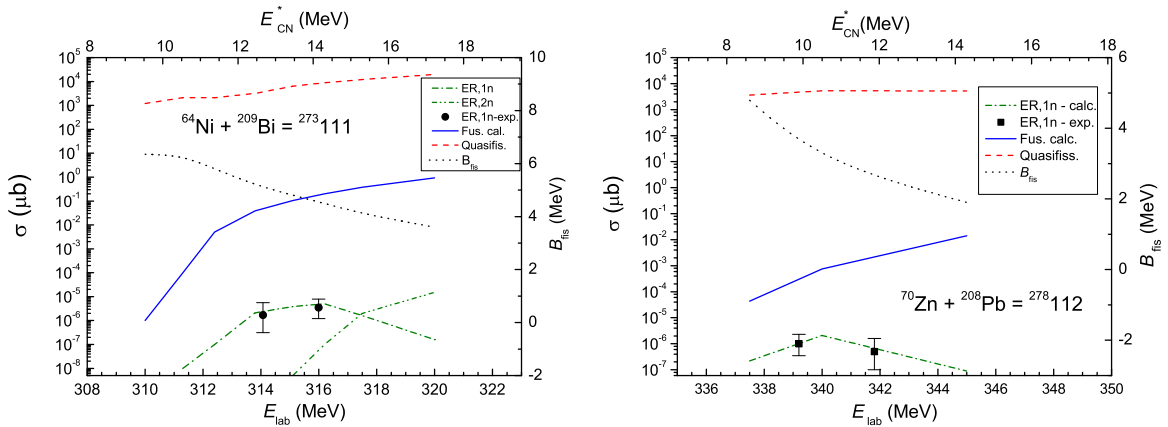


**Figure 10.** Comparison of the ER results (left scale) obtained by the DNS model (dot-dashed line) with the experimental data for the synthesis of Roentgenium and Copernicium in the  $^{64}\text{Ni}+^{209}\text{Bi}$  (left panel) and  $^{70}\text{Zn}+^{208}\text{Pb}$  (right panel) reactions, respectively. Quasifission and fusion excitation functions are shown by dashed and solid lines, respectively. The dotted line is the fission barrier (right scale).

## 5. Mixing of mass-angle distributions of the quasifission and fusion-fission products

The mass (charge) and angular distributions of the reaction products in the heavy ion collisions are the main indicator used to make conclusions about the reaction mechanism. According to the established opinion the products with masses close to the ones of projectile and target nuclei are considered as products formed in deep inelastic reactions; the products with the symmetric mass distributions are considered as products of the fusion-fission reactions, *i.e.* fission products of the heated and rotating compound nucleus formed at complete fusion; the products having intermediate masses between projectile-like and fusion-fission products are considered as quasifission products. The last kind of products appear when proton or neutron numbers in the heavy or light fragment are close to the magic numbers 28, 50, 82 or 126 [30, 31]. So, the symmetric mass distributions from capture reactions can either be the result of a compound nucleus formation followed by fission, or - if the criteria for compound decay are violated - they are ascribed to the quasifission and fast fission channels.

We should remind that quasifission products are formed in the decay of the DNS without reaching the stage of the compound nucleus or one can say without reaching the saddle point

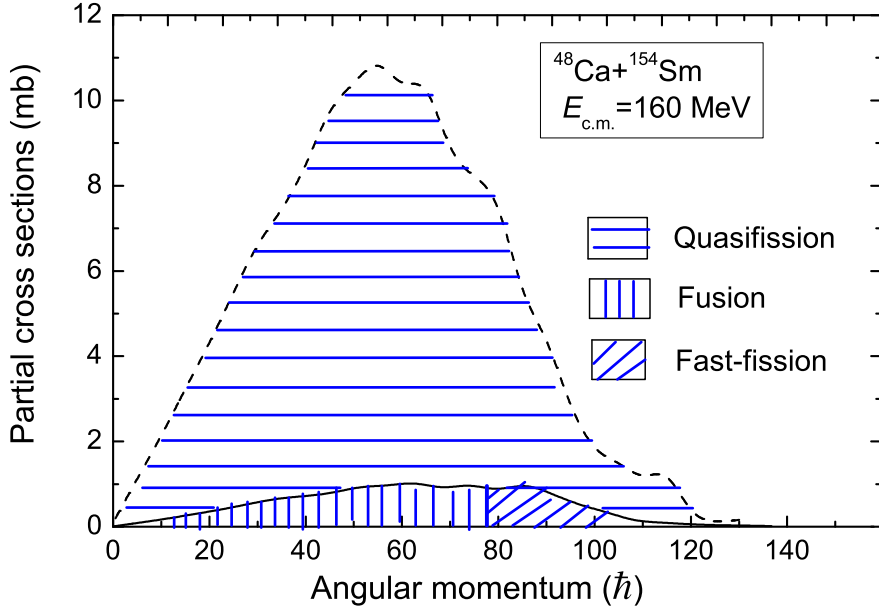


**Figure 11.** Partial cross sections (angular momentum distributions) of quasifission (area filled by the horizontal lines), fast fission (area filled by the skew-eyed lines) and complete fusion (area filled by the vertical lines) events calculated by the DNS model for the  $^{48}\text{Ca}+^{154}\text{Sm}$  reaction.

to arrive to the compact shape. Quasifission means that the TKE of binary fragments is close to that of fusion-fission products or Viola systematics.

The experimental methods used to estimate the fusion probability depend on the unambiguity of identification of the complete fusion reaction products among the quasifission products. The difficulties arise when the mass (charge) and angular distributions of the quasifission and fusion-fission fragments strongly overlap depending on the reaction dynamics. As a result, the complete fusion cross sections may be overestimated:

$$\sigma_{\text{fus}} = \sigma_{\text{ffis}} + \sigma_{\text{ER}}, \quad (18)$$

where  $\sigma_{\text{ER}}$  is measured by good accuracy while  $\sigma_{\text{ffis}}$  may include contribution of the quasifission and fast fission products which are formed in the decay of the DNS and in the decay of the deformed mononucleus-no compound nucleus. We remind the difference between quasifission and fast fission processes:

- Quasifission is the decay of DNS which is formed in the capture–full momentum transfer reactions. The angular momentum distribution for the quasifission events can extend from  $\ell = 0$  up to  $\ell = \ell_d$  where  $\ell = \ell_d$  the maximum value of the DNS angular momentum (see Fig. 11, area filled by the horizontal lines). The mass (charge) distribution of quasifission products may be in the wide range from masses (charges) of projectile- and target-like fragments up to symmetric masses mixing with the fusion-fission products.

- Fast fission is the decay of the mononucleus which is a non-equilibrated system survived against quasifission but unstable to be formed as compound nucleus due to the absence of a fission barrier caused by its fast rotational velocity [32]. Therefore, the partial cross section of fast fission is only populated at large values of the angular momentum  $\ell$  (see Fig.11, the area filled by skew-eyed lines).

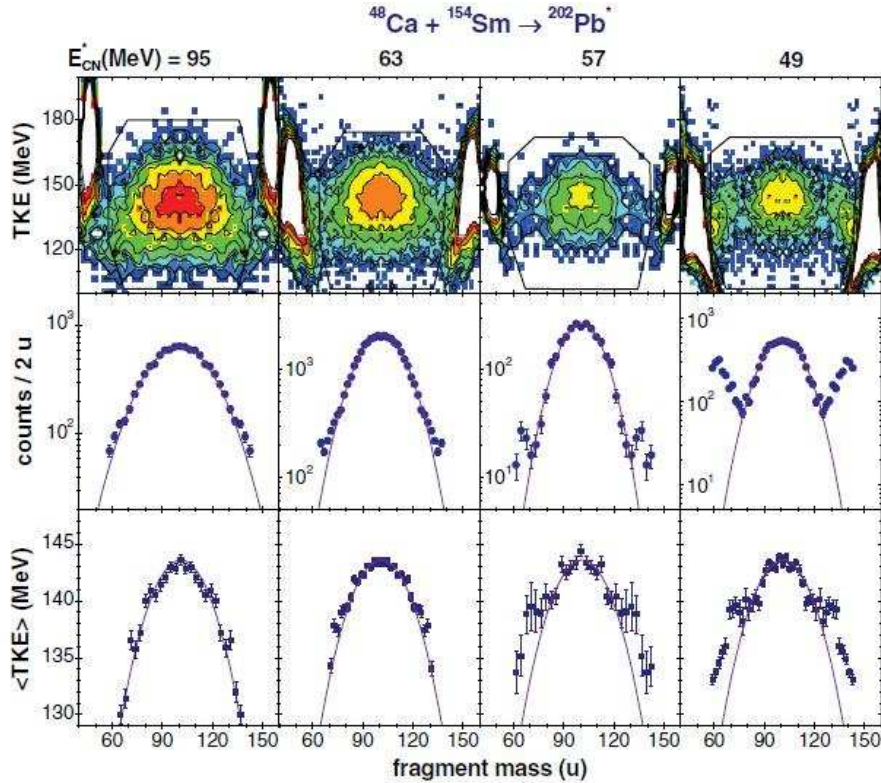


**Figure 12.** Two-dimensional TKEmass matrices (upper panels), yields of fragments and their TKE as a function of the fragment mass (middle and bottom panels, respectively) in the  $^{48}\text{Ca}+^{154}\text{Sm}$  reaction at different  $E_{\text{CN}}^*$  excitation energies (designated above the upper panels). Solid lines in the middle and bottom panels are Gaussian and parabola fits to the mass and TKE distributions, respectively. This figure was copied from Ref. [31].

We tried to analyze the reasons for the lack or disappearance of the quasifission feature in the experimental data of the  $^{48}\text{Ca}+^{144}\text{Sm}$  and  $^{48}\text{Ca}+^{154}\text{Sm}$  reactions presented in the paper [31] as the main conclusion of study. The authors established the fusion suppression and the presence of quasifission for the reactions with the deformed  $^{154}\text{Sm}$  target at beam energies near and below the Coulomb barrier. The ratio of the quasifission fragments with masses in the range  $55 < A < 145$  to the total mass distribution of fission fragments decreases, with respect to the contribution of the symmetric compound nucleus-fission, as the  $^{48}\text{Ca}$  projectile energy increases (see Fig. 12). The authors did not consider the possibility of quasifission product yield with masses outside the range  $55 < A < 145$ . The quasifission products are formed in the ranges  $A < 55$  and  $A > 145$  too. But those can be mixed with the products of deep inelastic reactions as in the  $^{48}\text{Ca}+^{208}\text{Pb}$  reaction which was discussed in Section 2. This is a reason why our theoretical results of the capture cross section (long dashed line) overestimated the

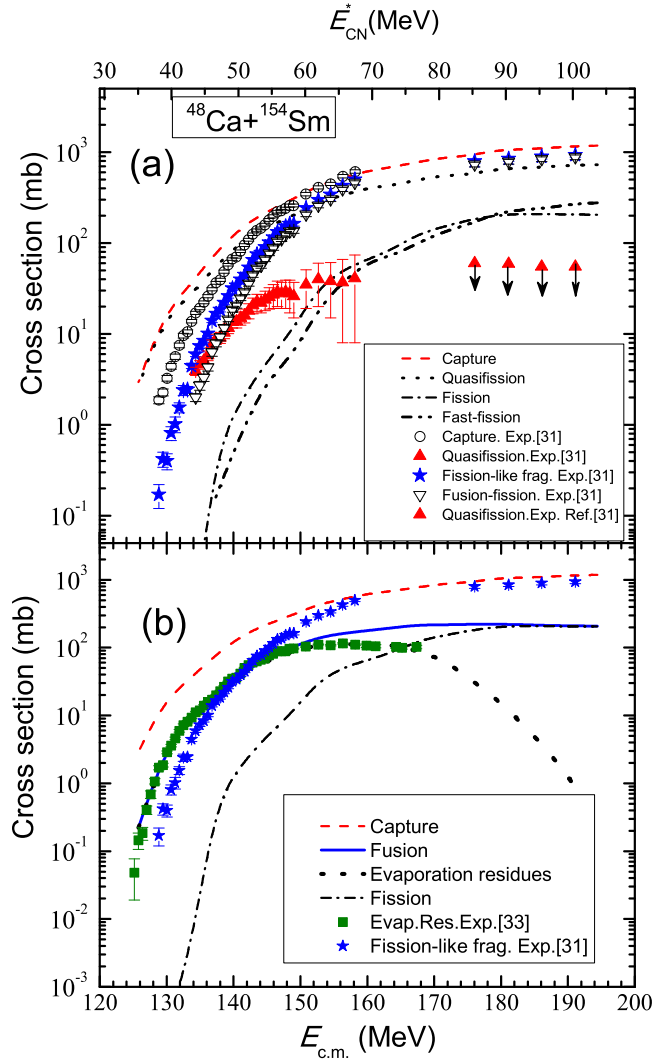


**Figure 13.** Comparison of the results of this work by the DNS model for the capture, complete fusion, quasifission, fast fission and evaporation residue cross sections with the measured data of the fusion-fission and quasifission given in Ref. [31] (panel (a)) and with data of the evaporation residues obtained from Ref. [33] (panel (b)) for the  $^{48}\text{Ca}+^{154}\text{Sm}$  reaction.

experimental data (open circles) presented in Ref. [31] at the low energies (see Fig. 13(a)).

The origin of the measured fission-like fragments (stars) at large bombarding energies is explained by the sum of the quasifission (short dashed line), fusion-fission (dash-dotted line) and fast fission (dash-double-dotted line) fragments (see Fig. neutrons and gamma-quanta 13). The cross section of the fast fission channel increases by increasing the bombarding energy due to the increase of the angular momentum of mononucleus. At low energies the contribution of the fusion-fission to the yield of binary fragments is small in comparison with the quasifission contribution. The small calculated fusion-fission cross section is explained by the large fission barrier ( $B_f=12.33$  MeV) for the  $^{202}\text{Pb}$  nucleus according to the rotating finite range model by A. J. Sierk [32] and by the additional barrier  $B_f^{(\text{micr})} = -\delta W = -(\delta W_{\text{saddle-point}} - \delta W_{\text{gs}}) \cong 8.22$  MeV caused by the nuclear shell structure. We conclude that the experimental fusion-fission data obtained at low energy collisions contain a huge contribution of quasifission fragments with

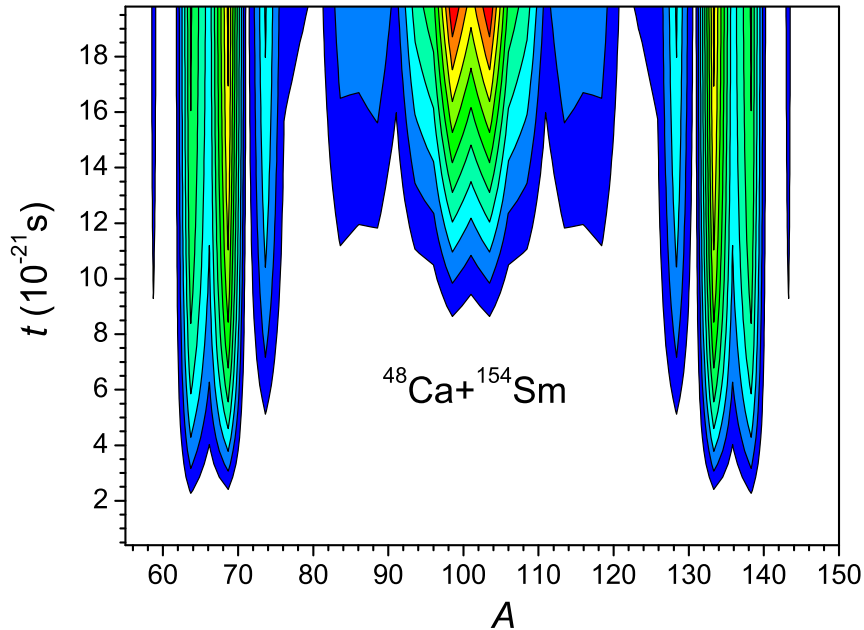


**Figure 14.** Mass distribution of quasifission products formed in the  $^{48}\text{Ca}+^{154}\text{Sm}$  reaction as a function of time.

masses  $A > 83$  which show an isotropic distribution as presented in Ref. [31]. This is not a new phenomenon and it was discussed as a result of theoretical studies, for example, in our previous papers [11, 34] and in Ref. [35]. The experimental results confirming this conclusion appeared recently in Ref. [36, 37]. The contribution of the mass symmetric products mixed with the fusion-fission products with similar masses increases the ambiguity of estimations of fusion cross section by formula (18). This is the reason for the difference between our theoretical results and the extracted ones from the experimental data for quasifission.

At the large energy  $E_{\text{c.m.}}=154$  MeV ( $E_{\text{CN}}^*=63$  MeV) the experimental values of the quasifission cross section are much lower than those of the fusion-fission cross section [31]. According to our theoretical result a sufficient part of the quasifission fragments shows the behaviour of fusion-fission fragments: the mass distribution can reach the mass symmetric region and their angular distribution can be isotropic due to the possibility that the dinuclear system rotates by large angles for large values of its angular momentum [38]. The authors of Ref. [31] did not exclude such a behaviour of the quasifission fragments. It is difficult to separate the quasifission fragments from the fusion-fission fragments when both, their mass and angle distributions, overlap in the region of symmetric masses. So, ignoring the quasifission products mixed with deep inelastic collisions and considering all the mass symmetric products as fusion-fission products give the reasons for the difference between the theoretical (dashed line in Fig. 13(a)) and experimental (up filled triangle in Fig. 13(a)) values of quasifission cross sections.

At low energies the projectile-like quasifission fragments with  $A < 70$  give a large contribution to the cross section for the considered  $^{48}\text{Ca}+^{154}\text{Sm}$  reaction since the excitation energy of the DNS is too small to shift the maximum of the mass distribution to more mass symmetric configurations of the DNS. The observed quasifission features at low energies are connected with the peculiarities of the shell structure of the interacting nuclei. The increase in the beam energy leads to a decrease of the shell effects and the yield of the quasifission fragments near the asymmetric shoulders decreases because the main contribution of quasifission moves to the

mass symmetric range. As it is seen from Fig. 14, the yield of products with the masses in the range  $85 < A < 125$  appears at times  $t > 8.5 \cdot 10^{-21}$  s. The evaporation residue and fusion-fission excitation function were calculated by the advanced statistical model [39, 40]. In this model, the partial fusion cross sections obtained by the DNS model were used as input data.

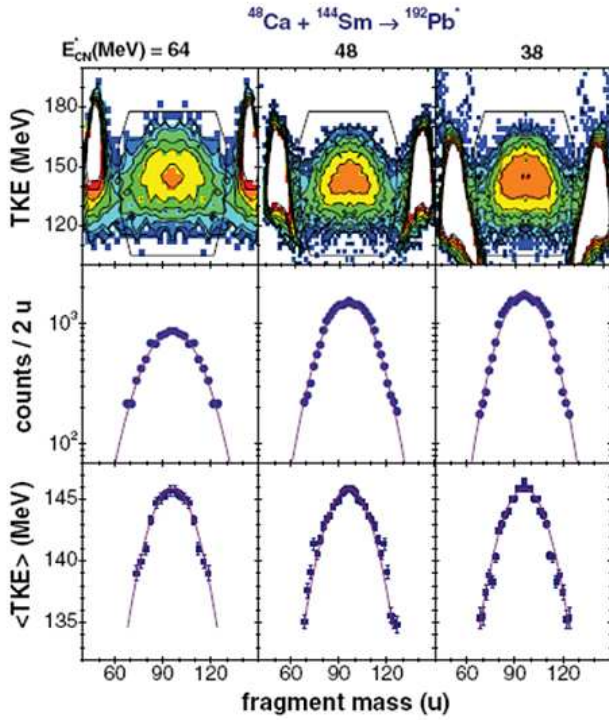


**Figure 15.** Two-dimensional TKEmass matrices (upper panels), yields of fragments and their TKE as a function of the fragment mass (middle and bottom panels, respectively) in the  $^{48}\text{Ca} + ^{144}\text{Sm}$  reaction at the different  $E_{\text{CN}}^*$  excitation energies (designated above the upper panels). Solid lines in the middle and bottom panels are Gaussian and parabola fits to the mass and TKE distributions, respectively. This figure was copied from Ref. [31].

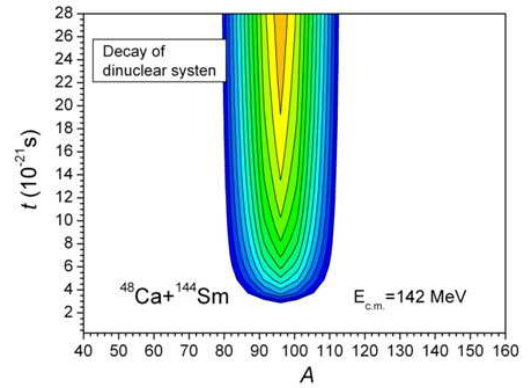


**Figure 16.** The mass distribution of the quasifission products formed in the  $^{48}\text{Ca} + ^{144}\text{Sm}$  reaction as a function of time.

Due to large fission barriers of the compound nucleus  $^{202}\text{Pb}$  the fission probability is very small and the yield of the evaporation residues after neutron emission cascade dominates. Therefore, our theoretical fission excitation function (dot-dashed line) presented in Fig. 13(a) is sufficiently lower than the experimental data (down open triangles). As we have discussed above the latter data included a contribution of the quasifission events. It is important to note that the evaporation residue excitation function (thick dotted line in Fig. 13(b)) is in good agreement with the experimental data (solid squares in Fig. 13(b)) which is the unambiguous physical quantity obtained from Ref. [33]. This fact confirms the correctness of our partial fusion cross sections.

## 6. Conclusions

The difficulties in the identification of the quasifission products are connected with absence of the appropriate knowledge about the reaction mechanism and a complete analysis of the yields

of quasifission and accompanying particles. The assumption about the possibility to observe the yield of quasifission products only in the mass range in the middle between projectile-like and fusion-fission products is not completely true: if there is no sufficient yield of reaction products in this intermediate region it does not mean that there is no yield of the quasifission products. For example, the authors of Ref. [31] came to the same conclusion about the  $^{48}\text{Ca}+^{144}\text{Sm}$  reaction where they did not observe the characteristic peak of the quasifission products in the mass distribution (see Fig. 15). Our theoretical results of the charge and mass distributions show that there are two reasons of a lack of the usual quasifission peak: (i) one part of the mass distribution of the quasifission fragments is in the mass range of projectile-like products  $48 < A < 60$ ; (ii) another part of the quasifission fragments is mixed with the fusion-fission fragments and has similar isotropic distributions. The isotope  $^{144}\text{Sm}$  is a magic nucleus with the neutron number  $N=82$ . Therefore, the concentration of the asymmetric mode of the quasifission fragments in the mass range  $48 < A < 60$  is explained by the effect of the shell structure of the double magic projectile-nucleus  $^{48}\text{Ca}$  and magic target-nucleus  $^{144}\text{Sm}$  on the mass distribution of the reaction fragments. As a result, the mass distributions of the products of deep-inelastic collisions and asymmetric quasifission overlap in this mass range. This case is similar to the  $^{48}\text{Ca}+^{208}\text{Pb}$  reaction where the presence of the quasifission feature is doubtful. But our investigation shows that due to the collision of the double magic  $^{48}\text{Ca}$  and  $^{208}\text{Pb}$  nuclei the mass distribution of the quasifission fragments is concentrated around the initial masses (see Fig. 2) because the potential energy surface has a local minimum in this region. In Fig. 16, we present the time dependence of the mass distribution of quasifission products of the  $^{48}\text{Ca}+^{144}\text{Sm}$  reaction. One can see that the mass numbers of the quasifission products are concentrated in the mass range  $80 < A < 110$  which overlaps completely with the mass range of fusion-fission products. In different from the  $^{48}\text{Ca}+^{154}\text{Sm}$  reaction, in the  $^{48}\text{Ca}+^{144}\text{Sm}$  reaction no yield of the quasifission products were found in the intermediate mass range where quasifission is usually observed.

The lack of quasifission events in the experimental studies of the  $^{48}\text{Ca}+^{144}\text{Sm}$  reaction, *i.e.* disappearance of quasifission events by increasing the beam energy, is connected with the measurement and analysis of the experimental data. More advanced experiments at different beam energies and reaction charge asymmetries must be performed by measuring neutrons and gamma-quanta in coincidence with the fission-like products. The results of such experiments should be analyzed by studying the different correlation functions of the observed quantities to distinguish quasifission features in the case that the mass-angle distributions of the quasifission and fusion-fission fragments strongly overlap in the mass symmetric region. We should have information about the angular momentum and excitation energy of the system going to fission (compound nucleus or DNS) additionally to the mass, angle and kinetic energy distributions of the fission fragments and the accompanying neutrons. The theoretical models must be enough perfect and they should have a small number of free parameters to make unambiguous conclusions about the reaction mechanism after a good description of the observed experimental data which are interpreted without additional assumptions.

## References

- [1] M. Wilpert, B. Gebauer, Th. Wilpert, W. von Oertzen, H.G. Bohlen, and J. Speer, Phys. Rev. C **51** (1995) 680.
- [2] G.G. Adamian, R.V. Jolos, A.K. Nasirov, A.I. Muminov, Phys. Rev. C **53** (1996) 871.
- [3] R.V. Jolos, A.K. Nasirov, G.G. Adamian, A.I. Muminov, Eur. Phys. J. A **8** (2000) 115.
- [4] G. Giardina, S. Hofmann, A.I. Muminov, and A.K. Nasirov, Eur. Phys. J. A **8** (2000) 205.
- [5] Yu.Ts. Oganessian *et al.*, Phys. Rev. C **70** (2004) 064609; Yu. Ts. Oganessian *et al.*, Phys. Rev. C **79** (2009) 024603.
- [6] S. Hofmann, Z. Phys. A **358** (1997) 125; S. Hofmann, Rep. Progr. Phys. **61**(1998) 639; S. Hofmann and G. Münzenberg, Rev. Mod. Phys. **72** (2000) 733.
- [7] K. Morita *et al.*, J. Phys. Soc. Jpn. **73** (2004) 2593; K. Morita *et al.*, J. Phys. Soc. Jpn. **76** (2007) 043201.
- [8] G. Fazio *et al.*, Phys. Rev. C **72** (2005) 064614.

- [9] V. E. Viola, K. Kwiatkowski, M. Walker, Phys. Rev. C **31** (1985) 1550.
- [10] J.G. Keller, B.B. Back, B.G. Glagola, D. Henderson, S.B. Kaufman, S.J. Sanders, R.H. Siemssen, F. Videback, B.D. Wilkins, A. Worsham, Phys. Rev. C **36** (1987) 1364.
- [11] A.K. Nasirov, G. Giardina, A.I. Muminov, W. Scheid and U.T. Yakhshiev, *Proc. Symposium Nuclear Clusters, Rauschholzhausen, Germany, 5-9 August 2002* (ed. R. V. Jolos and W. Scheid, EP Systema, Debrecen) (2003) p.415; Acta Physica Hungarica A **19** (2004) 109.
- [12] G. Fazio *et al.*, J. Phys. Soc. Jpn **72** (2003) 2509.
- [13] H.A. Kramers Physica **7** (1940) 284; V.M. Strutinsky, Phys. Lett. **B47** (1973) 121.
- [14] P. Grangé *et al.*, Phys. Rev. C **27** (1983) 2063; P. Grangé Nucl. Phys. A **428** (1984) 37c.
- [15] P. Fröbrich and G.R. Tillack, Nucl. Phys. A **540** (1992) 353.
- [16] G. Fazio, G. Giardina, A. Lamberto, R. Ruggeri, C. Saccà, R. Palamara, A.I. Muminov, A.K. Nasirov, U.T. Yakhshiev, F. Hanappe, Eur. Phys. J. A **19** (2004) 89.
- [17] A. Nasirov, A. Fukushima, Y. Toyoshima, Y. Aritomo, A. Muminov, Sh. Kalandarov, R. Utamuratov, Nucl. Phys. A **759** (2005) 342.
- [18] A.R. Jungmans, M. de Jong, H.-G. Clerc, A.V. Ignatyuk, G.A. Kudyaev, K.-H. Schmidt, Nucl. Phys. A **629** (1998) 635.
- [19] A.K. Nasirov, A.I. Muminov, R.K. Utamuratov, G. Fazio, G. Giardina, F. Hanappe, G. Mandaglio, M. Manganaro, and W. Scheid, Eur. Phys. J. A **34** (2007) 325.
- [20] G. Rudolf, A. Gobbi, H. Stelzer, U. Lynen, A. Olmi, H. Sann, R.G. Stockstad and D. Pelte, Nucl. Phys. A **330** (1979) 243.
- [21] G. Fazio, G. Giardina, G. Mandaglio, F. Hanappe, A.I. Muminov, A.K. Nasirov, W. Scheid, L. Stuttgé, Mod. Phys. Lett. A **20** (2005) 391.
- [22] E.V. Prokhorova *et al.*, Nucl. Phys. A **802** (2008) 45.
- [23] G. Audi, A.H. Wapstra, Nucl. Phys. A **595** (1995) 509.
- [24] P. Möller, J.R. Nix, Atom. Data and Nucl. Data Tabl. **39** (1988) 213.
- [25] N.A. Antonenko, E.A. Cherepanov, A.K. Nasirov, V.P. Permjakov, V.V. Volkov, Phys. Lett. B **319** (1993) 425; Phys. Rev. C **51** (1995) 2635.
- [26] J.P. Blocki, H. Feldmeier, W.J. Swiatecki, Nucl. Phys. A **459** (1986) 145.
- [27] G. Giardina, A.K. Nasirov, G. Mandaglio, F. Curciarello, V. De Leo, G. Fazio, M. Manganaro, M. Romaniuk and C. Saccà, Journal of Physics: Conference Series **282** (2011) 012006.
- [28] Ch. E. Düllmann, Phys. Rev. Lett. **104** (2010) 252701.
- [29] S. Heinz, V. Comas, S. Hofmann, D. Ackermann, J. Heredia, F.P. Heßberger, J. Khuyagbaatar, B. Kindler, B. Lommel and R. Mann, Journal of Physics: Conference Series **282** (2011) 012007.
- [30] M.G. Itkis *et al.*, Nucl. Phys. A **734** (2004) 136.
- [31] G.N. Knyazheva, E.M. Kozulin, R.N. Sagaidak, A.Yu. Chizhov, M.G. Itkis, N.A. Kondratiev, V. M. Voskressensky, M. Stefanini, B.R. Behera, L. Corradi, Phys. Rev. C **75** (2007) 064602.
- [32] A.J. Sierk, Phys. Rev. C **33** (1986) 2039.
- [33] A. M. Stefanini *et al.*, Eur. Phys. J. A **23** (2005) 473.
- [34] G. Fazio, G. Giardina, A. Lamberto, R. Ruggeri, F. Hanappe, T. Materna, U. Yu. Jovliev, A.V. Khugaev, A.I. Muminov, A.K. Nasirov *Proc. Int. Symposium "New Prospects and Lines of Research in Nuclear Physics", Messina, Italy, 24-26 October 2002*, ed. G. Fazio and F. Hanappe, World Scientific, Singapore (2003) p.258.
- [35] Y. Aritomo, M. Ohta, Nucl. Phys. A **744** (2004) 3.
- [36] D.J. Hinde, R. du Rietz, M. Dasgupta, R.G. Thomas, and L.R. Gasques, Phys. Rev. Lett. **101** (2008) 092701.
- [37] G. N. Knyazheva, M.G. Itkis, E.M. Kozulin, V.G. Lyapin, V.A. Rubchenya, V. Trsacka, S.V. Khlebnikov, Particles and Nuclei, Letters **5** (2008) 40 (in Russian).
- [38] A.K. Nasirov, A.I. Muminov, G. Giardina, G. Mandaglio, M. Manganaro, Journal of Physics: Conference Series **205** (2010) 012018.
- [39] A. D'Arrigo, G. Giardina, M. Herman and A. Taccone, Phys. Rev. C **46** (1992) 1437.
- [40] A. D'Arrigo, G. Giardina, M. Herman, A. V. Ignatyuk and A. Taccone, J. Phys. G **20** (1994) 365.